A study on sheet formability by a stretch-forming process using assumed strain FEM

K. Narooei · A. Karimi Taheri

Abstract The effects of sheet thickness and frictional condition between the punch and sheet on formability is predicted and compared with the experimental results of the Erichsen test as a stretch-forming process. The material and geometrical nonlinearity are considered. A hypoelastic–plastic model is used and strain-field stabilization is taken into account using the Assumed Strain Finite-Element Method. By considering the contact problem and applying the nonlinear finite-element method, the force and dome height for aluminum and steel sheets are computed and compared with the experimental results. The Oyane criterion is used to access the formability of the sheet. A good agreement was found between the experimental and predicted formability results of aluminum and steel sheets. The results show that for decreasing friction coefficient the position of tearing is moved from the rim to the pole. Also, by increasing the work-hardening exponent, formability is increased.

Keywords Erichsen test · FEM · Formability · Hypoelastic-plastic model · Stabilization

1 Introduction

Nowadays automotive industries tend to reduce the weight of components and body of cars. Hence, there is a tendency to reduce the thickness of sheets used in those industries and to increase their mechanical properties such as strength and formability [1]. Unfortunately, the tests used to assess the formability of sheets are destructive. Moreover, conducting a standard test to evaluate the formability is time consuming. Therefore, the finite-element method is being gradually adopted by industry to predict the formability of sheet metals [2].

Various methods have been used so far to model sheet-forming processes and formability. For example, Wang [3] has analyzed the deformation of circular sheet in a stretch-forming process with the FDS method using the stress equilibrium for a small element. Knibloe and Wagoner [4] simulated the hemispherical punch stretching experiments on an uncoated aluminum killed steel considering the sheet anisotropy and obtained best fits of experimental strain distributions using either a Hill quadratic [5] or non-quadratic criterion [6]. They assumed the Coulomb-friction

K. Narooei · A. Karimi Taheri (✉)
Department of Materials Science and Engineering, Sharif University of Technology, Azadi Ave., P.O. Box 11365-9466, Tehran, Iran
e-mail: ktaheri@sharif.edu

K. Narooei
e-mail: keyvan@mehr.sharif.ir

condition to be valid in their simulation. Lim et al. [7] attained the maximum cup height by a combination of stretching and drawing processes. They considered the process geometrical parameters and achieved the optimum cup height in their experiments. Reis et al. [8] utilized the DD3IMP code and solid finite elements to allow an accurate calculation of the stress gradients through the sheet thickness. They were able to determine the sheet thickness evolution in their work. It should be noted that, although these researchers used large elastoplastic strains and rotation in their model, the details of their code and constitutive equations are not clear. Evangelista et al. [9] took into account the modified Murciniak–Kuczyncki model and combined this method with the finite-element method. They have reported that their results show some deviation from the FLDs results presented in the literature. It seems that these deviations may be due to the shear stress in a real process which is not considered in the Murciniak–Kuczyncki model. Using the DYNA 3D finite-element code Mamalis et al. [10] simulated the stretch-forming process. They used isotropic material model and elastic–plastic behavior and found good agreement between the model and experiment.

Yang and Hsu [11] combined the elastic–plastic membrane finite-element and forming limit theory to determine the limiting dome height for an axisymmetric stretch-forming process. They used the criterion given by Yoshida et al. [12] as the formability criterion and reported that the larger the value of the strain-hardening exponent, the smaller the anisotropy parameter, and the lower the friction coefficient, the more uniform is the strain distribution.

Considering the literature and the above brief review it will be appreciated that meaningful work has been carried out on the simulation of the sheet-forming processes. However, to the authors' knowledge virtually no modeling has been carried out so far to evaluate sheet formability in a stretch-forming process using an assumed strain finite-element method. Therefore, in the present investigation a 3D simulation is performed to assess the effects of friction, thickness, and strain-hardening coefficient on sheet formability in a hemispherical punch-stretching process. Using the nonlinear finite-element method (updated Lagrangian formulation) in conjunction with solid elements, the nonlinearity due to material (elastic–plastic model) as well as the nonlinearity due to geometry and contact problem is taken into account. It should be mentioned that, although the solid elements are seldom used to analyze sheet forming processes, due to their enormous cost in terms of CPU time, as mentioned above in the cases where the stress gradient through sheet thickness or thickness change is needed, these elements must be used [8]. However, in order to overcome the highly nonlinear problem and mesh instability due to these elements, the assumed strain finite element is used in the analysis for the first time.

2 Nonlinear finite-element formulation

To formulate the process, the Hu–Washizu principle in weak form [13–15] is used here:

$$\int_\Omega \delta \bar{D} : \sigma(\bar{D}) \mathrm{d}\Omega + \int_\Omega \delta \left[\bar{\sigma} : \left(D\left(V\right) - \bar{D} \right) \right] \mathrm{d}\Omega - \delta p^{\mathrm{ext}} = 0, \tag{1}$$

where V is the velocity, $\bar{D}$ the assumed rate of deformation, and $\bar{\sigma}$ the assumed stress. Taking into account the Simo–Hughes assumption [15], which considers the normality of the assumed stress and the difference between the rate of deformation and the assumed rate of deformation, the second term of above equation is zero. Thus, Eq. 1 reduces to:

$$\{\bar{D}\} = \bar{B}\dot{d}, \quad f^{\mathrm{int}} = \int_\Omega \bar{B}^T \{\sigma(\bar{D})\} \mathrm{d}\Omega, \tag{2}$$

where, $\dot{d}$ is the nodal velocity vector, $\bar{B}$ a matrix defined at the center of the parent element, a superscript "T" shows the transpose of a matrix, and f^{int} denotes the internal nodal forces due to the stress field. Using a Taylor series expansion in bilinear terms [16,17] one obtains:

$$\bar{B} = B_a\left(0\right) + B_{a,\xi}\left(0\right)\xi + B_{a,\eta}\left(0\right)\eta + B_{a,\zeta}\left(0\right)\zeta + B_{a,\xi\eta}\left(0\right)\xi\eta + B_{a,\eta\zeta}\left(0\right)\eta\zeta + B_{a,\xi\zeta}\left(0\right)\xi\zeta, \tag{3}$$

$$B_a^T = \left[N_{a,x}(0) \quad N_{a,y}(0) \quad N_{a,z}(0) \right]. \tag{4}$$

Table 1 Permutation of i, j and k

i	j	k
1	2	3
1	3	2
2	1	3
2	3	1
3	1	2
3	2	1

Here "0" indicates the center of a parent element and it means that Eqs. 3 and 4 should be computed at the center of the parent element. The derivation of Eq. 3 is presented in [17]. Further ξ, η and ζ are the parent-element coordinates; N_a is the standard isoparametric shape function for an eight-node hexahedral element and subscripts after a comma show the derivative argument. In the components of Eqs. 3 and 4 the hourglass vector has been entered to eliminate the zero-energy mode associated with the one-point quadrature element that results in a non-constant strain field [16,18].

In order to prevent shear and volumetric locking, the strain operator $\bar{B}$ is decomposed into dilatational and deviatoric parts [17]:

$$\bar{B} = \bar{B}^{\text{dil}} + \bar{B}^{\text{dev}}. \tag{5}$$

To eliminate volumetric locking, the dilatational part is evaluated at the center of element as:

$$\bar{B}^{\text{dil}} = \bar{B}^{\text{dil}}(0). \tag{6}$$

To avoid shear locking, the deviatoric part is considered in an orthogonal co-rotational coordinate system defined as follows:

For each element a local coordinate system rotating with the element is considered, so that two tangent vectors in the mid-surface of a parent element located at $\xi = 0$ can be defined as;

$$g_1 = \begin{bmatrix} N_{I,\xi} x_I & N_{I,\xi} y_I & N_{I,\xi} z_I \end{bmatrix}_{\xi=0}, \quad g_2 = \begin{bmatrix} N_{I,\eta} x_I & N_{I,\eta} y_I & N_{I,\eta} z_I \end{bmatrix}_{\xi=0}. \tag{7}$$

The unit vectors of the co-rotational coordinate system are calculated from Eq. 7 as;

$$\hat{e}_1 = \frac{\frac{g_1}{\|g_1\|} + \frac{g_2}{\|g_2\|}}{\left\| \frac{g_1}{\|g_1\|} + \frac{g_2}{\|g_2\|} \right\|}, \quad \hat{e}_2 = \hat{e}_3 \times \hat{e}_1, \quad \hat{e}_3 = \frac{g_1 \times g_2}{\|g_1 \times g_2\|}. \tag{8}$$

Then, the transformation matrix is taken as;

$$R = \begin{bmatrix} \hat{e}_1 \\ \hat{e}_2 \\ \hat{e}_3 \end{bmatrix}. \tag{9}$$

The coordinate in the co-rotational system, $\hat{x}$, can be obtained using the transformation rule:

$$\hat{x} = Rx. \tag{10}$$

To avoid shear locking, the deviatoric part is considered in the above orthogonal co-rotational coordinate system as:

$$\bar{B}_{ii}^{\text{dev}} = \bar{B}_{ii}^{\text{dev}}(0) + \bar{B}_{ii,\xi}^{\text{dev}}(0)\xi + \bar{B}_{ii,\eta}^{\text{dev}}(0)\eta + \bar{B}_{ii,\zeta}^{\text{dev}}(0)\zeta + \bar{B}_{ii,\xi\eta}^{\text{dev}}(0)\xi\eta + \bar{B}_{ii,\eta\xi}^{\text{dev}}(0)\eta\xi + \bar{B}_{ii,\xi\zeta}^{\text{dev}}(0)\xi\zeta, \tag{11}$$

$$\bar{B}_{ij}^{\text{dev}} = B_{ij}^{\text{dev}}(0) + B_{ij,\xi_k}^{\text{dev}}(0)\xi_k. \tag{12}$$

In Eq. 12 the indices i, j, and k are permuted as given in Table 1.

By substituting $\bar{B}$ in Eq. 2 the volumetric and shear locking are removed. Then, displacement, strain, and stress fields can be calculated by applying the material and contact models to Eq. 2 as follows.

2.1 Material model

A rate-independent elastic–plastic material that obeys Von Mises plasticity is chosen as the material model. For simplicity the isotropic hardening and associative flow rule will be considered. The yield criterion function f of Von Mises can be written as:

$$f\left(\sigma, \bar{\varepsilon}, \sigma_y\right) = \left[\frac{3}{2} S : S\right]^{0.5} - \sigma_y\left(\varepsilon\right), \quad S = \sigma - \frac{1}{3}\text{tr}\left(\sigma\right) I, \tag{13}$$

where S is the deviatoric stress, I the unity tensor, tr() the trace operator, $\bar{\varepsilon}$ the effective strain, and σ_y the yield stress. By additive decomposition of the strain the following equation is obtained:

$$\dot{\sigma} = C^e : \left(\dot{\varepsilon} - \dot{\varepsilon}^p\right), \tag{14}$$

where C^e is the fourth-order elastic-modulus tensor. According to the normality and associative flow rules, the plastic strain-rate vector is normal to the yield surface [13,19]. Therefore:

$$n = \frac{\frac{\partial f}{\partial \sigma}}{\left\|\frac{\partial f}{\partial \sigma}\right\|} = \frac{S}{\|S\|}. \tag{15}$$

The plastic strain rate can be calculated from the following formula:

$$\dot{\varepsilon}^p = \dot{\lambda} r, \tag{16}$$

$$r = \frac{3S}{2\left[\frac{3}{2} S : S\right]}, \quad \dot{\lambda} = \frac{r : C^e : \dot{\varepsilon}}{H + r : C^e : r}, \tag{17}$$

where H represents the work-hardening rate. Replacing for $\dot{\lambda}$ in Eq. 16 from Eq. 17 and then for $\dot{\varepsilon}^p$ in Eq. 14 from Eq. 16, the value of $\dot{\sigma}$ is determined using the following relation:

$$\dot{\sigma} = C : \dot{\varepsilon}, \tag{18}$$

where C is the elastic–plastic tensor defined as:

$$C_{ijkl} = \lambda^e \delta_{ij}\delta_{kl} + G(\delta_{ik}\delta_{jl} + \delta_{il}\delta_{jk}) - 2G\frac{1}{1 + \frac{H}{3G}} n_{ij} n_{kl}, \tag{19}$$

where λ^e is the first Lamé parameter and G is the shear modulus. In order to take into account the work-hardening effect of the material in the model, a radial return algorithm composed of two steps is considered. In the first step an elastic trial stress is computed from the solution of the last time step. In the second step, if the trial stress lies outside the yield surface, it will be projected to the closest point on the yield surface. On the other hand, both the expansion of the yield surface and the appropriate plastic strain or strain rate are taken into account. Figure 1 shows the flow chart for the determination of the plastic strain.

2.2 Contact model

To model the contact between the punch, die rim, and the sheet a penalty-based formulation is considered [20]. It is assumed that the friction force is proportional to the normal force. Thus:

$$\phi = \|P_T\| - \mu_f \|P_N\|, \tag{20}$$

where μ_f indicates the friction coefficient, P_T the tangential force and P_N the normal force. Similar to the stress updating mentioned above, an elastic force is estimated as:

$$P_{n+1}^{\text{trial}} = P_n + D \cdot u_{n+1}, \tag{21}$$

where subscripts show the increment number. Finally, in order to satisfy Eq. 20, a correction term [21] defined by Eq. 22 is added to Eq. 21:

$$P_{T_{n+1}} = \mu_f \left\|P_{N_{n+1}}^{\text{trial}}\right\| T_{n+1}, \quad T_{n+1} = \frac{P_{T_{n+1}}^{\text{trial}}}{\left\|P_{T_{n+1}}^{\text{trial}}\right\|}. \tag{22}$$

2.3 Tangent stiffness matrix and nodal force vector

In order to achieve the stiffness matrix and nodal force vector the isoparametric shape function of eight node hexahedral element will be used. It is worth mentioning that this type of element is preferred to the shell element which cannot accurately predict the variation in thickness as a significant parameter in the tearing phenomenon.

From the shape function, the displacement and velocity can be defined as:

$$\Delta u = N \Delta d, \tag{23}$$

$$V = N \dot{d}. \tag{24}$$

Assuming the Green–Naghdi rate [17] and linearization of Eq. 2, we get:

$$\hat{K}^{\nu} \Delta d = \hat{r}^{\nu+1} = \hat{f}_{\text{ext}}^{\nu+1} - \hat{f}_{\text{int}}^{\nu}, \tag{25}$$

$$\hat{K}^{\nu} = \int_{\Omega} \hat{\bar{B}}^{T} \hat{C}^{\nu} \hat{\bar{B}} d\Omega + \int_{\Omega} \hat{\bar{B}}^{T} \hat{T} \hat{\bar{B}} d\Omega, \tag{26}$$

$$\hat{f}_{\text{int}}^{\nu} = \int_{\Omega} \hat{\bar{B}}^{T} \hat{\sigma}^{\nu} d\Omega, \tag{27}$$

where $\hat{K}^{\nu}$ indicates the stiffness matrix, ν the iteration number, $\hat{f}_{\text{int}}^{\nu}$ and $\hat{f}_{\text{ext}}^{\nu+1}$ are the internal and external nodal forces. The first term in Eq. 26 represents the material stiffness matrix and the second term is the geometric stiffness matrix. Note that the above integrations are carried out in the co-rotational coordinate system. After performing the above integrals and before the assemblage step all variables are transformed to the global coordinate system using the transformation matrix defined by Eq. 9. To do so one obtains:

$$K^{\nu} = R^{\nu T} \hat{K}^{\nu} R^{\nu}, \qquad r^{\nu+1} = R^{\nu T} \hat{r}^{\nu+1}. \tag{28}$$

It should be noted that the tangent stiffness matrix due to the nonlinearity of the contact (Eq. 29), defined by Peric and Owen [20], should be added to the above stiffness matrices.

$$D^{ep} = -K_{T}^{*} \left(I - T_{n+1} \otimes T_{n+1} - N_{n+1} \otimes N_{n+1} \right) - \mu_{f} K_{N} \left(T_{n+1} \otimes N_{n+1} \right) - K_{N} \left(N_{n+1} \otimes N_{n+1} \right),$$

$$K_{T}^{*} = K_{T} \frac{P_{T_{n+1}}}{\left\| P_{T_{n+1}} \right\|}; \tag{29}$$

here N_{n+1} and T_{n+1} denote the normal and tangential unit vectors in the contact area. Finally, to solve Eq. 25, the modified Newton–Raphson algorithm is used and the predicted results of the punch force are compared with experiment.

3 Experiments

Using the DIN 50101 standard [22], we conducted Erichsen's test to measure the formability of 1050 aluminum and mild-steel sheets of 0.5 and 1 mm thickness, respectively. Square specimens of 90×90 mm were cut from the sheets. The specimens were stretched until either a macroscopic localization or a sudden reduction in force was observed. In this set-up the depth of the punch was measured as the Erichsen index (IE) to identify sheet formability. The schematic diagram of die set used in this test is shown in Fig. 2:

Three kinds of lubrication consisting of; (1) dry ($\mu = 0.3$), (2) nylon as lubricant ($\mu = 0.14$), and (3) lubrication by grease ($\mu = 0.21$) were used in the tests. Regarding the standard, we applied a minimum amount of blank holder force of 9800 N on the specimen. A tensile test was carried out in one direction to establish the effective stress-versus-strain relationship of the sheet materials described by Eqs. 30 and 31 for the aluminum and steel sheets, respectively. Therefore, no anisotropy was considered in the current work.

$$\text{Al} : \bar{\sigma} = 110 \bar{\varepsilon}^{0.24} \tag{30}$$

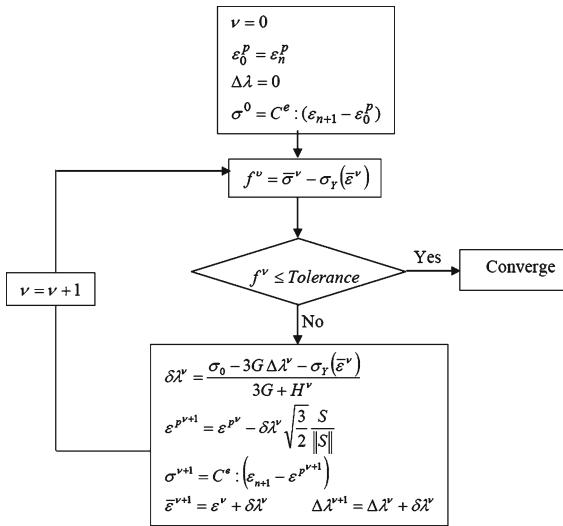$$\text{St} : \bar{\sigma} = 987.41 \bar{\varepsilon}^{0.486} \tag{31}$$

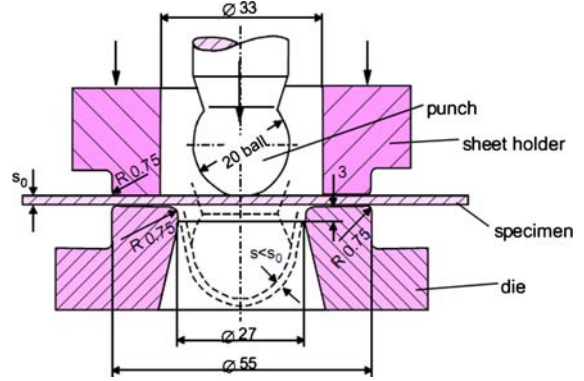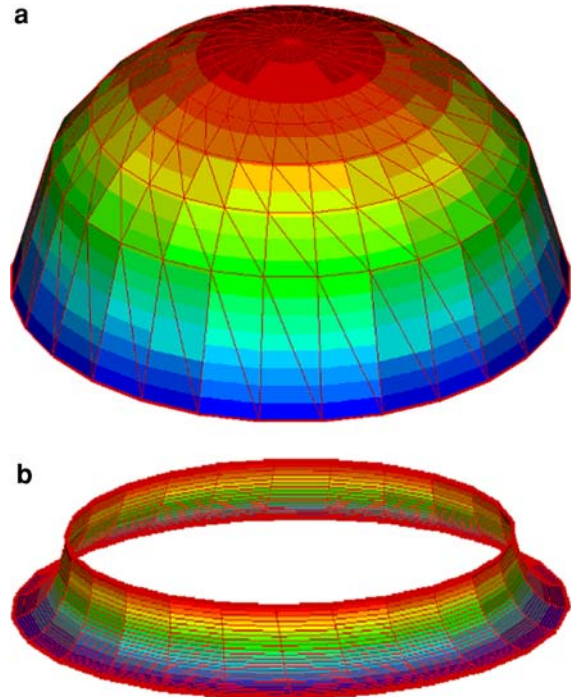**Fig. 1** The flowchart for calculating the plastic strain

Fig. 2 The schematic of the Erichsen die set

Fig. 3 a Punch. **b** Die rim

4 Results and discussion

The geometry used for the punch and die rim are shown in Fig. 3. Note that these meshes are used only to represent the punch and die rim. For the computation of the normal unit vector in the contact algorithm the geometry of the punch and die rim is used. In the simple geometry situation the normal vector is defined as:

$$N = \frac{\nabla g}{|\nabla g|}, \tag{32}$$
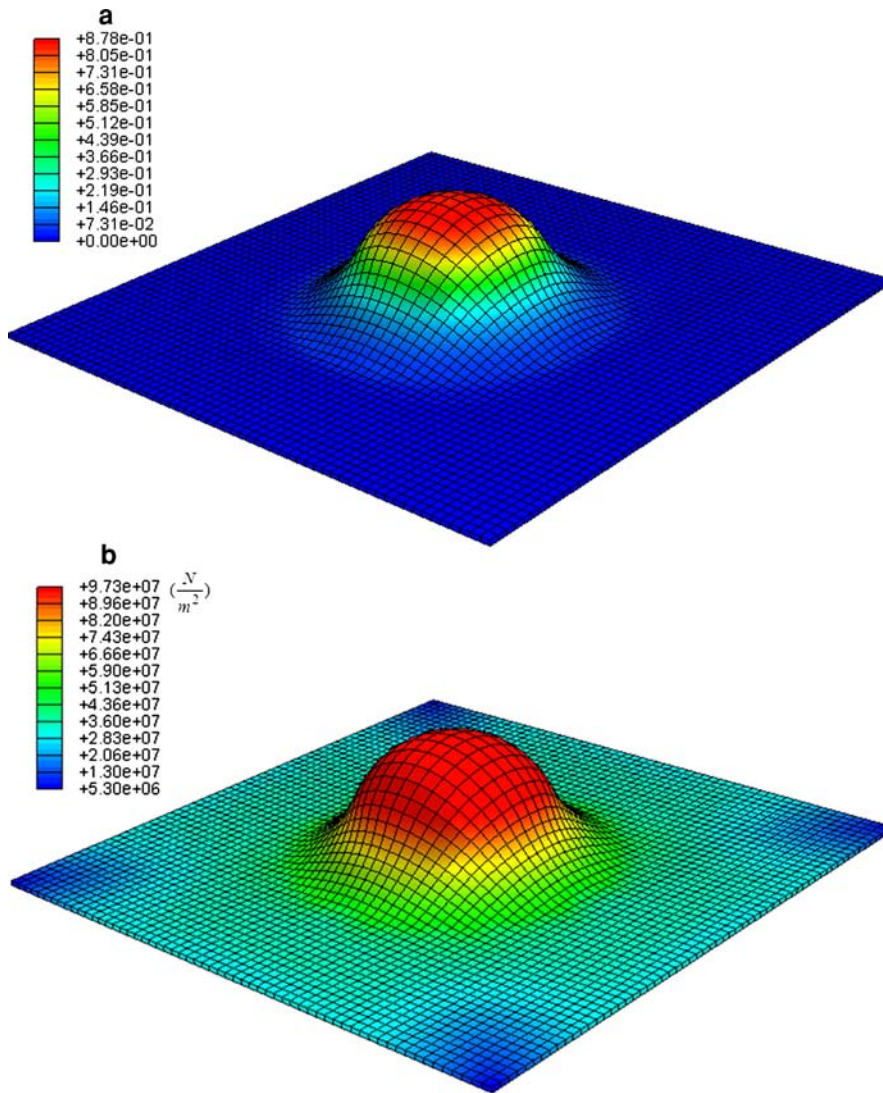
Fig. 4 **a** Effective strain. **b** Stress contour of aluminum sheet using nylon as lubricant

where the function g represents the geometry of a rigid punch or die rim and the symbol "∇" is the gradient operator. Also, $g \leq 0$ represents the contact condition for nodes on a sheet with punch or die rim. So, here the smoothing algorithm or fining of the rigid-body (punch or die rim) mesh in finite sliding is not necessary. In doing so, the computational cost is reduced and contact constraint is imposed more accurately.

As the sheet is stretched, a localized flow takes place at a point of the sheet leading eventually to sheet tearing. This phenomenon is considered here to evaluate sheet formability. In other words, the punch depth at the tearing instance was taken as the formability index. Therefore, a criterion should be utilized to monitor when tearing or localization occurs. In this research the Oyane criterion [21,23] is used as a warning of the failure instance:

$$\int_0^{\varepsilon_f} \left(\frac{\sigma_m}{\bar{\sigma}} + C \right) \mathrm{d}\bar{\varepsilon} = D, \tag{33}$$

where σ_m is the hydrostatic stress and $\bar{\sigma}$ and $\bar{\varepsilon}$ are the effective stress and strain, respectively. Further, ε_f is the fracture strain in a uniaxial tensile test and C and D are constants relating to material properties ($C = -0.36$ and

Fig. 5 The deformed specimen after performing the Erichsen test on aluminum sheet using nylon as lubricant
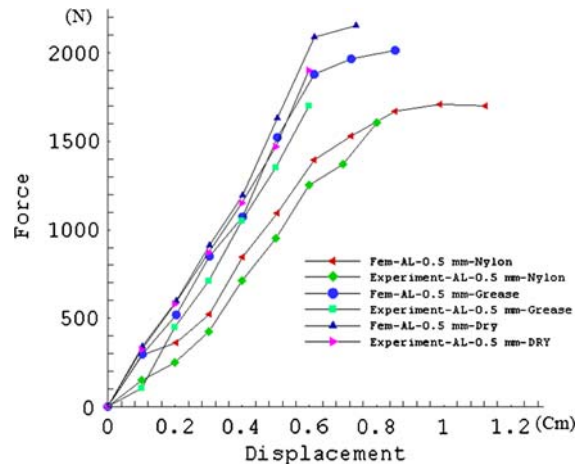

Fig. 6 Force-displacement curve for aluminum sheet with different lubricant

$D = 0.24$ for mild steel and $C = 0.33$ and $D = 0.42$ for aluminum [24]). Simulation of hemispherical punch stretching was carried out by computing at each node and for each increment the left-hand side of Eq. 32, so as to detect the attainment of tearing. Hence, the deformation contour of a specimen is determined when Eq. 32 is satisfied.

The contour of effective strain and stress of the aluminum sheet using nylon as the lubricant between the punch and die are shown in Fig. 4. The effective stress unit in this figure and the subsequent figures is given in Pascals. As the contours show, the stress is monotonically raised from the die rim to the pole and accordingly the strain is increased towards the pole. Note that the stretching state of stress prevails and because of the good lubrication, the material prefers to stretch and slide over the punch. The punch force was measured as 1600 N and the punch stroke as 0.75 cm. Figure 5 exhibits the experimentally stretched specimen. As can be seen, the failure has occurred in the vicinity of the pole. The predicted strain and stress contour also indicates that the minimum of thickness and the maximum of stress have occurred in this region. (Note that where strain is high the thickness is low, because the sheet is in a stretched state and, with increasing element length, a reduction in thickness occurs.) Referring to Fig. 4, we observe that the minimum-thickness position coincides with the maximum strain and, because of the work-hardening in this position, the maximum effective stress is attained.

In Fig. 6 the force-displacement curve is presented. It is observed that a good correlation exits between the experiment and the FEM results. To consider the effect of friction on the formability of the aluminum sheet, the grease lubricant was also applied. The respective punch load versus the punch movement is shown in Fig. 6. Compared with the results presented for the nylon lubricant the punch load has increased by changing the lubricant from nylon to grease. In this condition the force was measured as 1700 N and the punch stroke as 0.6 cm. Figure 7 shows the deformed sheet. The predicted contours of the effective strain and stress of the sheet are shown in Fig. 8. It is interesting to note that the failure occurs far from the pole compared with lubrication by nylon. This behavior is confirmed by the FEM contour. Moreover, a minor reduction in the dome height and a major increase in the stress level are observed using grease instead of nylon as lubricant. This confirms the results reported by Knibloe and Wagoner utilizing membrane elements and the FEM approach [4].

To further investigate the effect of friction, the Erichsen test was conducted without any lubrication (dry condition) on the same aluminum sheet material. Figure 9 exhibits the predicted contours of the effective strain and stress of the sheet. The force was measured as 1900 N and the punch stroke as 0.6 cm. Figure 10 exhibits the experimental results of the Erichsen test performed on the sheet. In Fig. 6 the force-displacement curve for the dry state is also presented. Referring to Fig. 6 we see that by increasing the friction coefficient the force-stroke curve exhibits a

Fig. 7 The deformed
specimen after performing
the Erichsen test on
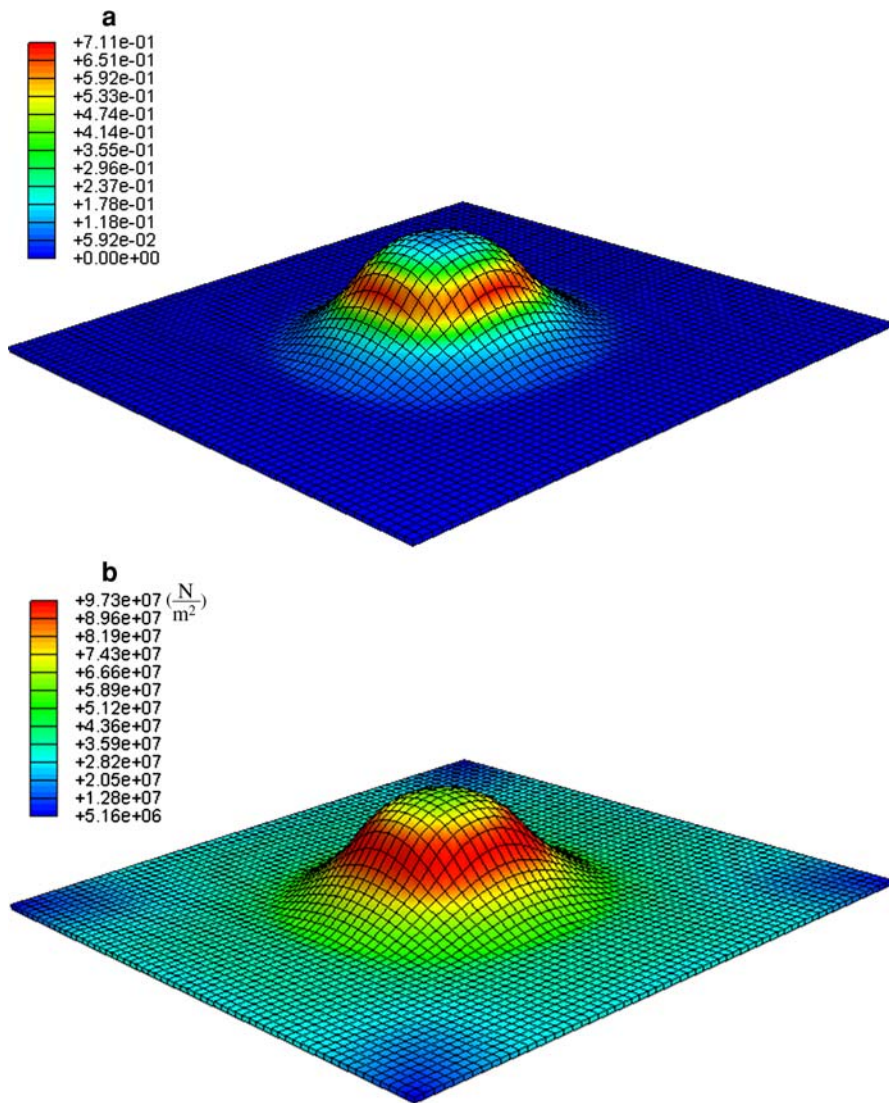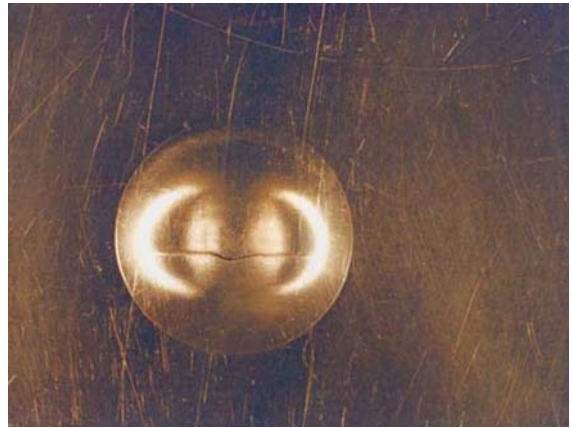aluminum sheet using
grease as lubricant

Fig. 8 **a** Effective strain. **b** Stress contour of aluminum sheet using grease as lubricant
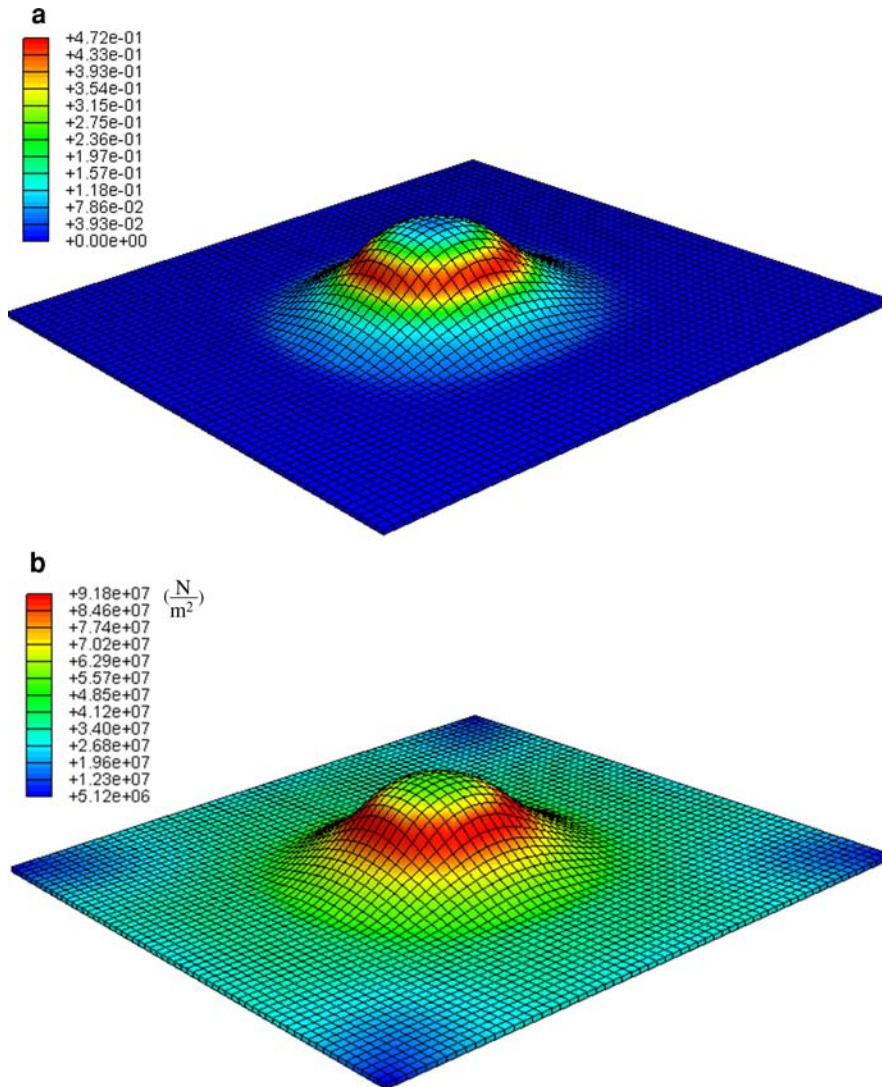
Fig. 9 **a** Effective strain. **b** Stress contour of aluminum sheet without lubricant

linear variation. To investigate this behavior, the code was run with friction modeling $\tau = mK$ where m is the friction factor. As is observed for high μ-values, a good correlation between these two friction models is achieved [25]. Therefore, one can conclude that for high friction the use of the $\tau = mK$ model in sheet forming does not cause a problem. Also, referring to Figs. 5, 7 and 10, we observe that by increasing the friction coefficient, the position of the tearing moves to a further distance from the pole because at high friction the material prefers to clamp the punch while the other parts that do not have any contact with the punch prefer to stretch.

In order to assess the effect of the material property on the IE index, steel sheet of 0.5 mm thickness was also tested using the Erichsen die set. Figure 11 exhibits the experimental results. In this experiment the punch force was measured as 12.1 KN and the punch stroke as 1 cm. The predicted force-displacement relating to this condition is shown in Fig. 12.

Figure 13 shows the predicted contours of the effective strain and stress of the steel sheet with a nylon lubricant. As can be seen the failure occurs in the vicinity of pole. Also, this position presents the minimum thickness and the maximum stress. A more uniform distribution of thickness and stress causes a uniform tearing to be observed
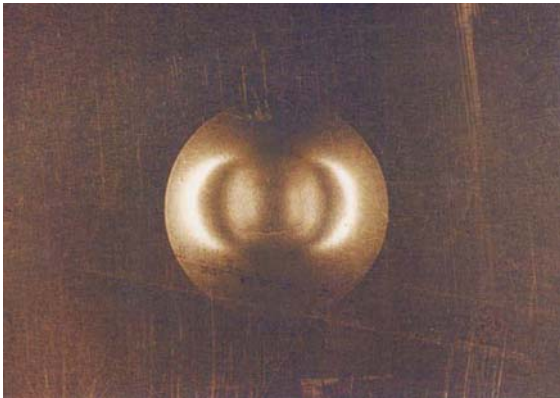
Fig. 10 The deformed specimen after performing the Erichsen test on aluminum sheet without lubricant
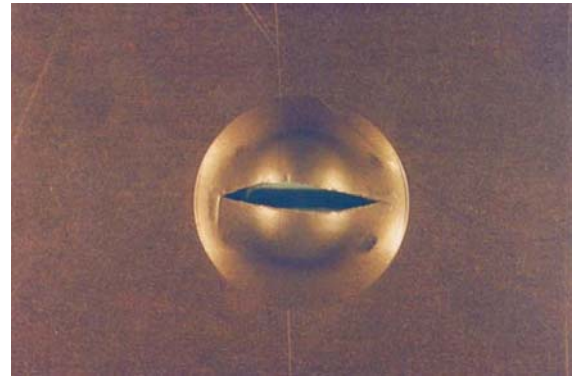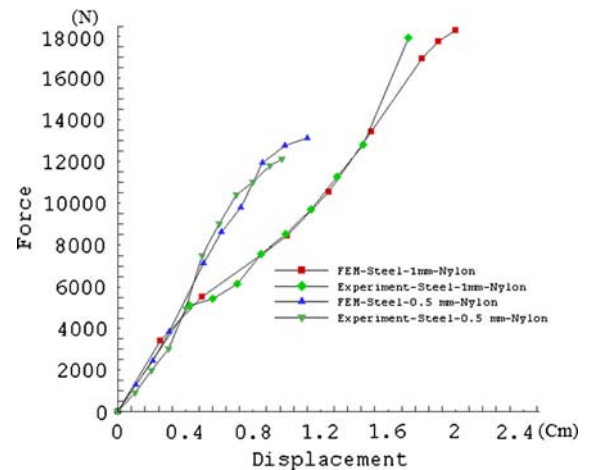

Fig. 11 The deformed specimen after performing the Erichsen test on steel sheet using nylon as lubricant (thickness = 0.5 mm)

Fig. 12 Force-displacement curve for steel sheet with different thickness and nylon as lubricant

in the pole. To compare the results presented in Fig. 6 with those in Fig. 12, these results are combined in Fig. 14. It is found that, by increasing the strain-hardening exponent, the IE index is increased by about 40% for the same frictional condition. Also, comparing the results presented in Figs. 4a and 13a it is observed that the steel sheet has a more uniform strain and thickness after stretching compared with the Al sheet. This phenomenon can be attributed to the higher strain-hardening exponent of steel compared to that of an Al sheet.

In order to investigate the thickness effect on the IE index, a steel sheet of 1 mm thickness was used in the Erichsen test. Figure 15 shows the contour of the effective strain and stress of the sheet using nylon as lubricant.

The force was measured as 18300 N and the punch stroke as 2 cm. Figure 16 exhibits the experimental results. As can be seen for a two-fold increase in thickness, the IE index increases by a factor of two as well (Fig. 12). Comparing the predicted and the experimental results of punch force versus punch displacement, it is clear that the Oyane criterion in predicting the dome height presents a better agreement for the steel sheet.

5 Conclusion

In this study a FEM model for predicting the formability of sheet metals in a stretching stress state has been developed. For removing the major drawback of mesh instability, an assumed strain FEM was used. To use the advantages of the implicit method a special case of the contact problem with penalty method was included. The
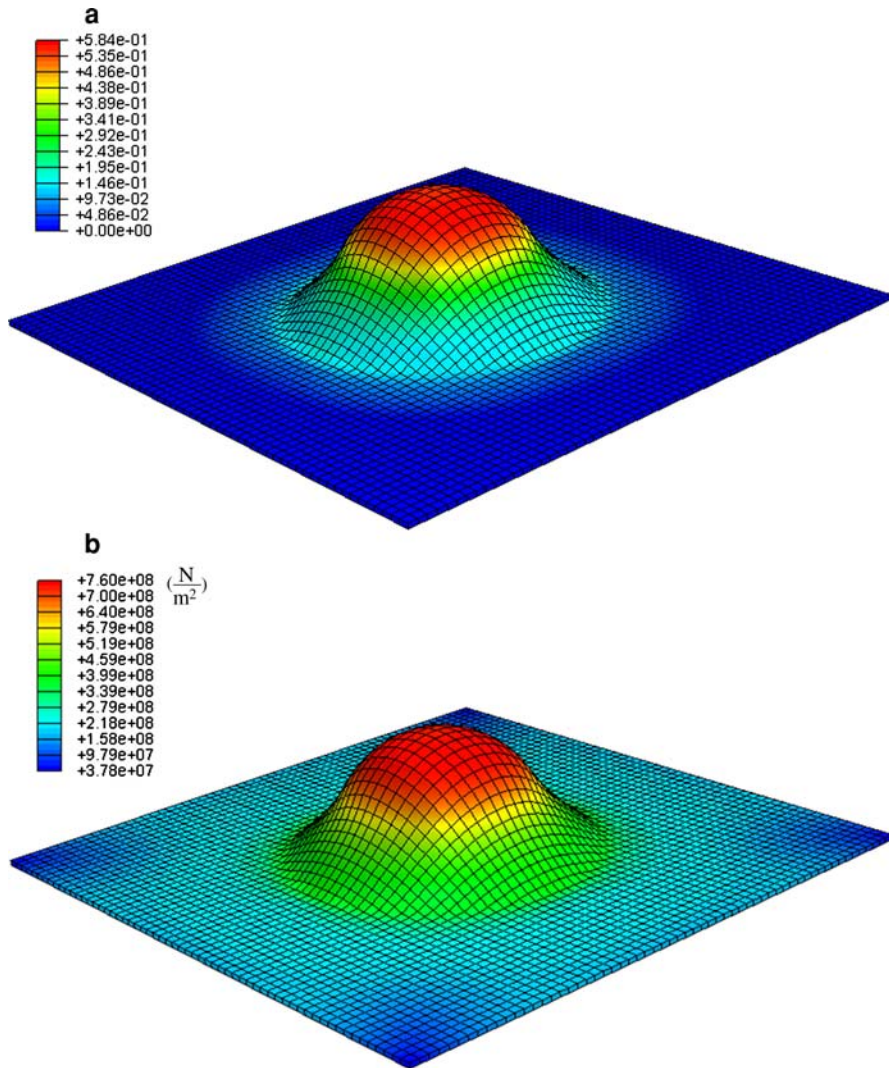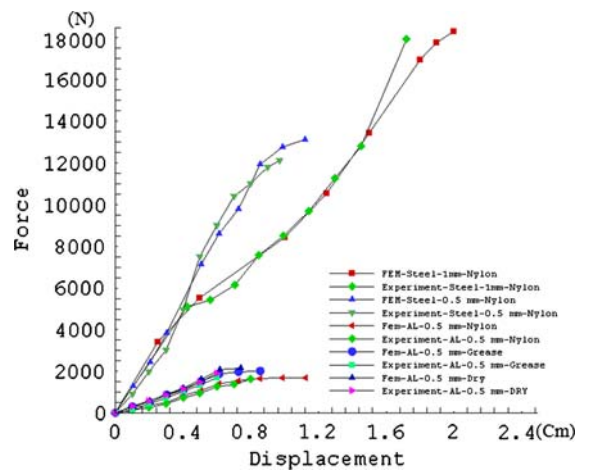
Fig. 13 **a** Effective strain. **b** Stress contour of steel sheet using nylon as lubricant (thickness = 0.5 mm)

Fig. 14 Force-displacement curve for steel and aluminum sheets using different lubricant and thickness
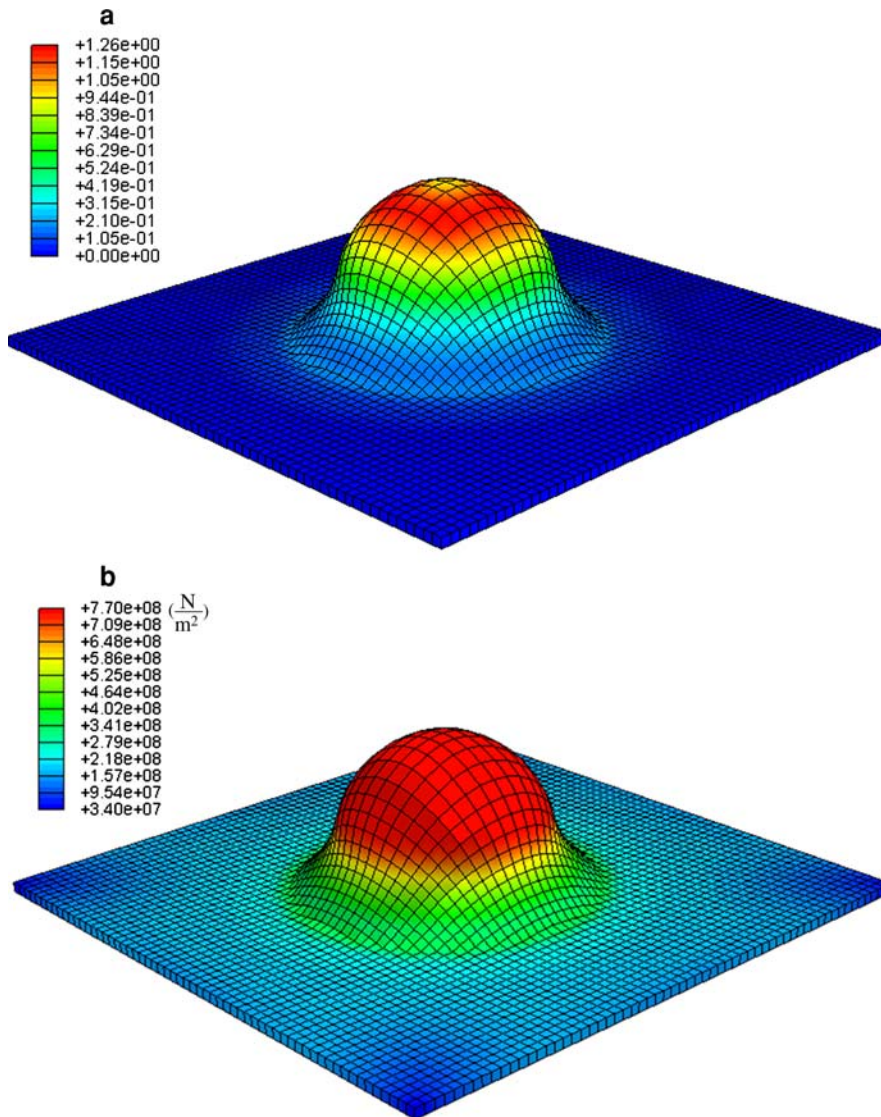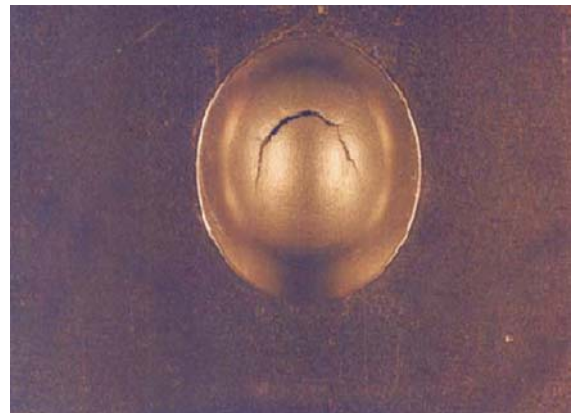
Fig. 15 **a** Effective strain. **b** Stress contour of steel sheet using nylon as lubricant (thickness = 1 mm)

Fig. 16 The deformed specimen after performing the Erichsen test on steel sheet using nylon as lubricant (thickness = 1 mm)

predicted results showed good agreement with experiment. From the results we conclude that the strain-hardening exponent and ductility have a significant influence on sheet formability. Also, with increasing sheet thickness the formability is increased, although it does not act as a controlling parameter. Moreover, the lubricants used in this work did not show a major effect on sheet formability.

References

1. Uthaisangsuk V, Prahl U, Munstermann S, Bleck W (2008) Experimental and numerical failure criterion for formability prediction in sheet metal forming. Comput Mater Sci 43(1):43–50
2. Fan JP, Tang CY, Tsui CP, Chan LC, Lee TC (2006) 3D finite element simulation of deep drawing with damage development. Int J Mach Tool Manuf 46:1035–1044
3. Wang NM (1970) Large plastic deformation of a circular sheet caused by punch stretching. J Appl Mech 37:431–440
4. Knibloe JR, Wagoner RH (1989) Experimental investigation and finite element modeling of hemispherically stretched steel sheet. Metall Mater Trans A 20:1509–1521
5. Hill R (1948) A theory of the yielding and plastic flow of anisotropic metals. Proc R Soc Lond A, 193:281–297
6. Hill R (1979) Theoretical plasticity of textured aggregates. Math Proc Camb Philos Soc, 85:179–191
7. Lim TC, Ramakrishna S, Shang HM (2000) Simultaneous stretch forming and deep drawing in axisymmetrical sheet forming. J Mater Process Technol 97:82–87
8. Santos AD, Reis A, Duarte JF, Teixeira P, Rocha AB, Oliveira MC, Alves JL, Menezes L (2004) A benchmark for validation of numerical results in sheet metal forming. J Mater Process Technol 155(156):1980–1985
9. Evangelista SH, Lirani J, Al-Qureshi HA (2002) Implementation a modified Marciniak-Kuczynski model using the finite element method for the simulation of sheet metal deep drawing. J Mater Process Technol 130–131:135–144
10. Mamalis AG, Manolakos DE, Baldoukas AK (1997) Finite-element modeling of the stretch forming of coated steels. J Mater Process Technol 68:71–75
11. Yang T-S, Hsu T-C (2001) Forming limit analysis of hemispherical-punch stretch forming. J Mater Process Technol 117:32–36
12. Yoshida T, Katayama T, Usuda M (1995) Forming-limit analysis of hemispherical-punch stretching using the three-dimensional finite-element method. J Mater Process Technol 50:226–237
13. Belytschco T, Liu WK, Moran B (2000) Nonlinear finite element for continua and structures. Wiley, New York, 455 pp
14. Flanagan DP, Belytschco T (1981) A uniform strain hexahedral and quadrilateral with orthogonal hourglass control. Int J Numer Methods Eng 17:679–706
15. Simo JC, Hughes TJR (1986) On the variational foundations of assumed strain methods. Trans ASME J Appl Mech 53(1):51–54
16. Belytschco T, Bindeman L (1993) Assumed strain stabilization of the eight node hexahedral element. Comput Methods Appl Mech Eng 105(2):225–260
17. Liu WK, Guo Y, Tang S, Belytschco T (1998) A multiple quadrature eight node hexahedral finite element for large deformation elastoplastic analysis. Comput Methods Appl Mech Eng 154:69–132
18. Belytschco T, Ong J, Liu WK, Kennedy JM (1984) Hourglass control in linear and nonlinear problem. Comput Methods Appl Mech Eng 43:251–276
19. Khan A, Hung S (1995) Continuum theory of plasticity. Wiley, New York
20. Peric DJ, Owen DRJ (1992) Computational model for 3-D contact problem with friction based on the penalty method. Int J Num Meth Eng 35:1289–1309
21. Fromentin S, Martiny M, Ferron G, Tourki Z, Moreira LP, Ferran G (2001) Finite element simulation of sheet metal forming processes for planar anisotropic materials. Int J Mech Sci 43(8):1833–1852
22. DIN 50101 (1979) Erichsen cupping test on sheet and strip metal
23. Oyane M (1972) Criteria of ductile fracture strain. Bull Jpn Soc Mech Eng (JSMN) 15:1507–1513
24. Takuda H, Mori K, Jinno A, Hatta N (1996) Finite element simulation of redrawing processes with ductile fracture criterion. In: Abe T, Tsuta T (eds) Proceedings of the third AEPA'96. Pergamon, Hiroshima, 691 pp
25. Matuszak A (2000) Factors influencing friction in steel sheet forming. J Mater Process Technol 106:250–253